

Latent Structure Emergence in Diffusion Models via Confidence-Based Filtering

Wei Wei ^{*1} Yizhou Zeng ^{*1} Kuntian Chen ¹ Sophie Langer ² Mariia Seleznova ³ Hung-Hsu Chou ^{*1}

Abstract

Diffusion models rely on a high-dimensional latent space of initial noise seeds, yet it remains unclear whether this space contains sufficient structure to predict properties of the generated samples, such as their classes. In this work, we investigate the emergence of latent structure through the lens of confidence scores assigned by a pre-trained classifier to generated samples. We show that while the latent space appears largely unstructured when considering all noise realizations, restricting attention to initial noise seeds that produce high-confidence samples reveals pronounced class separability. By comparing class predictability across noise subsets of varying confidence and examining the class separability of the latent space, we find evidence of class-relevant latent structure that becomes observable only under confidence-based filtering. As a practical implication, we discuss how confidence-based filtering enables conditional generation as an alternative to guidance-based methods.

1. Introduction

Diffusion models (Sohl-Dickstein et al., 2015; Ho et al., 2020) and their variations (Rombach et al., 2022; Song et al., 2023) have achieved remarkable success, yet their internal structure remains only partially understood. In particular, the relationship between the initial noise seeds in the latent space and their corresponding generated samples is poorly characterized. Recent work, such as Xu et al. (2025), has shown that selecting particular seeds can greatly improve the quality of generated images, highlighting the importance of understanding the latent structure underlying diffusion-based generation.

A major difficulty in this analysis is the stochasticity of the sampling process. In stochastic samplers such as DDPM,

generation depends not only on the initial noise seeds but also on additional noise injected at intermediate steps, obscuring the correspondence between latent variables and generated samples. In contrast, deterministic diffusion models such as DDIM (Song et al., 2021) allow an one-to-one relation between seeds and their corresponding samples. Consequently, to facilitate a cleaner analysis we focus on DDIM and the following questions:

1. Can properties of generated samples (e.g., class labels) be predicted from their initial seeds?
2. Does such predictability reflect nontrivial structure in the latent space?

We find that both questions admit affirmative answers when we focus on seeds and samples associated with higher classifier confidence, with the class label as the property of interest. In particular, filtering seeds by confidence reveals that high-confidence seeds are more predictable in terms of their class labels and exhibit clearer structure in the latent space. These observations suggest that diffusion models encode class-relevant structure that becomes apparent only through confidence-based filtering.

Moreover, the principles highlighted in this work suggest a new approach to conditional generation based on confidence-based filtering. The method trains a confidence function and a classifier on seeds, and generates samples only from the ones that is both high-confidence and belongs to the desired class. This approach requires no modification nor retraining of the diffusion model, treating it as a black box, and hence provides a different perspective on conditional generation beyond standard guidance-based methods.

We summarize our contributions as follows:

- We show that certain properties of a generated sample can be predicted from its initial seed prior to generation. This predictability is strong for high-confidence seeds and weak for low-confidence seeds, suggesting that high-confidence seeds exhibit more pronounced structure while low-confidence seeds are largely uninformative.

¹Department of Mathematics, University of Pittsburgh, USA

²Faculty of Mathematics, Ruhr-Universität Bochum, Germany

³Department of Mathematics, Ludwig-Maximilians-Universität München, Germany.

- We investigate the latent-space structure induced by confidence-based filtering and observe strong class separability for high-confidence seed, in contrast to little or no separability for low-confidence seed. This structural distinction helps explain the enhanced predictability associated with high-confidence seed.
- We demonstrate how these observations motivate a prototype conditional generation method that does not require modifying or retraining the underlying generative model. We further discuss its strengths, limitations, and potential, and outline directions for future research.

For notational simplicity, we refer to the initial noise seed simply as noise or seed throughout the paper.

2. Related Work

Several works aim to improve diffusion sampling by studying or shaping the intermediate representation induced by diffusion models. One line of work modifies latent spaces during training to impose desirable geometric and semantic properties. For instance, Diffusion Autoencoders (Preechakul et al., 2022) combine diffusion probabilistic models with autoencoder architectures to induce latent spaces that become progressively disentangled as noise increases, such that nearby latent points increasingly correspond to semantically similar samples. A similar approach is proposed by Cho et al. (2024), who learn two disentangled latent spaces simultaneously: one capturing structural or content-related features and another modeling global semantic attributes.

In more recent work, reward-based sampling has been used to improve image generation by aligning quality metrics (Lin et al., 2024), user preferences (Kirstain et al., 2023) or other reward signals (Kim et al., 2025). In this direction, Yeh et al. (2025) introduce Demon, a training-free inference-time method that optimizes the sampling noise itself to align pretrained diffusion models with arbitrary (possibly non-differentiable) reward functions. By iteratively resampling and scoring noise configurations, Demon biases the denoising trajectory toward high-reward regions. While related in spirit, our approach differs in that it uses a classifier to assign confidence scores to regions of the latent space, enabling targeted sampling without optimizing noise trajectories.

Another line of work aims to control the sampling process itself. One possible way is to guide the generation process by the gradient of a pre-trained classifier to achieve condition generation, which is called the Classifier Guidance (Dhariwal & Nichol, 2021). Li et al. (2022) combined Classifier Guidance with a pre-trained Transformer language model for text-to-image generation, and Wallace et al. (2023) improved this guidance method by directly optimizing diffusion latent variables. This idea goes beyond conditional

generation. For instance, Kim et al. (2023) uses discriminators to guide pretrained score-based diffusion models towards more realistic samples. More recently, Diffusion Rejection Sampling (DiffRS), introduced by Na et al. (2024), interprets the reverse diffusion process as an approximate sampler and uses a time-dependent discriminator to perform rejection sampling at each denoising step, yielding samples closer to the true data distribution.

An alternative approach is to embed the labels in the training phase, and use a classifier-free guidance (CFG) (Ho & Salimans, 2022; Nichol et al., 2021). Some recent improvements include the CFG++ model (Chung et al., 2024) that addresses mode collapse, the adaptive guidance (Castillo et al., 2023) enabling faster generation, and more theoretical interpretations of CFG (Bradley & Nakkiran, 2024; Pavasovic et al., 2025).

Unlike existing methods that modify denoising steps, our approach selects latent regions prior to sampling, without altering the reverse diffusion dynamics.

3. Background and Formulation

3.1. Diffusion Model Preliminaries

Let \mathcal{D} and $\mathcal{Z} \sim \mathcal{N}(0, I)$ be a data distribution and a latent distribution on \mathbb{R}^d , respectively. A standard diffusion model can be viewed as reversing a diffusion process $x_t : [0, T] \rightarrow \mathbb{R}^d$ that evolves from $x_0 \sim \mathcal{D}$ to $x_T \sim \mathcal{Z}$, and is described by the SDE

$$dx_t = \mu(t, x_t) dt + \sigma(t) dw_t, \quad (1)$$

where w_t denotes a Wiener process.

In the distributional sense, by the Fokker–Planck equation, this SDE is equivalent to the ODE

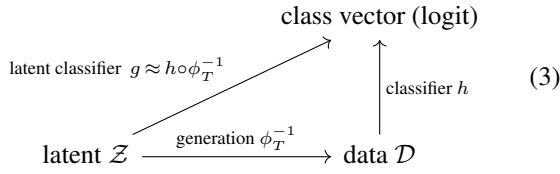
$$dx_t = \left(\mu(t, x_t) - \frac{1}{2} \sigma(t)^2 \nabla \log p_t(x_t) \right) dt, \quad (2)$$

where $p_t(x)$ is the probability flow induced by x_t , providing a deterministic counterpart of (1). For example, in the variance-preserving diffusion process, i.e. $\mu(t) = \frac{1}{2}\beta(t)$ and $\sigma(t) = \sqrt{\beta(t)}$, reversing the above stochastic and deterministic formulations yields DDPM (Ho et al., 2020) and DDIM (Song et al., 2021), respectively. However, although DDPM and DDIM share the same distribution, their particle trajectories differ substantially. In particular, under DDIM each initial noise seed deterministically corresponds to a unique generated sample, whereas this correspondence does not hold for DDPM due to additional stochasticity injected at intermediate sampling steps. Consequently, predictability is well defined only for DDIM, which is therefore the focus of our study.

3.2. Latent Classification

Let $\phi_T^{-1} : \mathbb{R}^d \rightarrow \mathbb{R}^d$ denote a deterministic diffusion model mapping an initial seed to its corresponding generated sample (the motivation for this notation will become clear shortly), and let $h : \mathbb{R}^d \rightarrow \mathbb{R}^C$ be a pretrained classifier, where C is the number of classes and the c -th entry of $h(x)$ represents the probability that x belongs to class c . For notation simplicity, we denote $[C] = \{1, \dots, C\}$.

To answer Question 1 in Section 1, we need to determine whether the composition $h \circ \phi_T^{-1}$ admits an efficient surrogate g acting directly on the latent space, such that $g \approx h \circ \phi_T^{-1}$ while avoiding the cost of evaluating the full generative map ϕ_T^{-1} , as illustrated in (3).



Due to the isotropic nature of the latent distribution, which lacks preferred directions, it may initially appear difficult to extract class information directly from the latent space without generating the corresponding sample. However, from the ODE perspective, such prediction is not only possible but also uniquely determined under suitable regularity assumptions.

Lemma 3.1. *Suppose*

$$F(t, x) := \mu(t, x) - \frac{1}{2}\sigma(t)^2 \nabla \log p_t(x) \quad (4)$$

is continuous on $[0, T] \times \mathbb{R}^d$ and locally Lipschitz in x , uniformly in t . Then (2) admits a unique regular flow map $\phi_t(x) : [0, T] \times \mathbb{R}^d \rightarrow \mathbb{R}^d$, i.e.,

$$\begin{cases} \frac{d}{dt} \phi_t(x) = \mu(t, \phi_t(x)) - \frac{1}{2}\sigma(t)^2 \nabla \log p_t(\phi_t(x)), \\ \phi_0(x) = x. \end{cases} \quad (5)$$

Then the corresponding probability flow $p_t(x)$ satisfies

$$p_t(x) = |\det(\nabla \phi_t^{-1}(x))| p_0(\phi_t^{-1}(x)). \quad (6)$$

In particular we have

$$\mathcal{Z}(x_T) = |\det(\nabla \phi_T^{-1}(x_T))| \mathcal{D}(\phi_T^{-1}(x_T) = x_0). \quad (7)$$

Given that ϕ_T^{-1} is well-defined, we can now examine how it transforms the latent distribution into the data distribution for each class. Let $D := \text{supp } \mathcal{D}$ denote the (closed) support of \mathcal{D} and decompose it according to $D = \bigcup_{c \in [C]} D_c$, where each D_c represents the support region of each class. We are interested in how D_c transforms under the flow map.

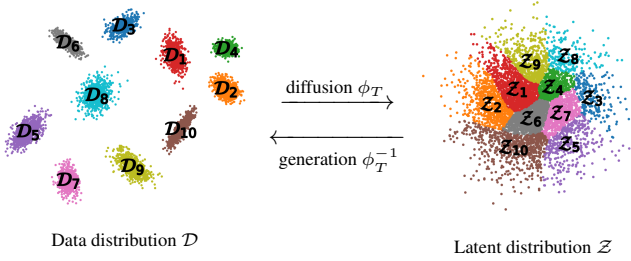


Figure 1. Correspondence of data classes and latent classes

Definition 3.2 (Data and latent class). The *data classes* $\{\mathcal{D}_c\}_{c \in [C]}$ and the *latent classes* $\{\mathcal{Z}_c\}_{c \in [C]}$ associated with \mathcal{D} are defined as

$$\mathcal{D}_c := \mathcal{D}(\cdot | D_c), \quad \mathcal{Z}_c := \mathcal{Z}(\cdot | Z_c) \quad (8)$$

where $Z_c := \phi_T(D_c)$.

By Theorem 3.1 one obtains the following theorem.

Theorem 3.3. *Let $Z := \text{supp } \mathcal{Z}$. Then Z admits the decomposition $Z = \bigcup_c Z_c$, and*

$$\mathcal{Z}_c = |\det \circ \nabla \phi_T^{-1}| \mathcal{D}_c \circ \phi_T^{-1} \quad (9)$$

is an explicit function based on \mathcal{D}_c and ϕ_T^{-1} . Moreover, if each D_c is connected and the sets $\{\mathcal{D}_c\}_{c \in [C]}$ are mutually disjoint, then so are Z_c and the sets $\{\mathcal{Z}_c\}_{c \in [C]}$.

In other words, if the diffusion model admits a unique regular flow transporting \mathcal{D} to the latent distribution \mathcal{Z} , then the same flow transports each \mathcal{D}_c to a corresponding latent class distribution \mathcal{Z}_c . Each \mathcal{Z}_c is supported on the region $Z_c = \phi_T(D_c)$, and together these regions form a decomposition of the latent support Z . Therefore identifying the function g is equivalent to identifying the regions Z_c .

3.3. Confidence-Based Filtering

In practice, learning over the entire latent space is challenging because the induced latent classes \mathcal{Z}_c 's can substantially overlap when the assumption in Lemma 3.1 fails. A key obstruction arises from the potential blow-up of the score $\nabla \log p_t$ in low-density regions, which can destroy the local Lipschitz regularity of the vector field F in (4) and invalidate standard uniqueness results for the flow map ϕ_t . When uniqueness fails, ϕ_t may become non-injective and hence not globally invertible. Consequently, the pushforward class densities \mathcal{D}_c to \mathcal{Z}_c may develop singularities, reflecting the mass concentration—or *mixing phenomenon*—observed in Section 5, making the learning of g in (3) infeasible.

To mitigate this issue, we introduce *confidence-based filtering*. Rather than attempting to invert the flow map globally, we restrict attention to regions of the latent space in which

the flow map exhibits well-behaved dynamics. We identify such regimes using a notion of confidence, and find that higher-confidence samples and their corresponding seeds are associated with more stable behavior.

Definition 3.4 (Label and confidence of seed). Let $h : \mathbb{R}^d \rightarrow \mathbb{R}^C$ to be a classifier mapping a sample to its logit. Define the label function $h_{\text{cls}} : \mathbb{R}^d \rightarrow [C]$ and confidence function $h_{\text{conf}} : \mathbb{R}^d \rightarrow [0, 1]$ as

$$h_{\text{cls}}(x) := \arg \max_c h_c(x) = c^* \quad (10)$$

$$h_{\text{conf}}(x) := h(x)_{c^*} - \max_{c \neq c^*} h(x)_c. \quad (11)$$

The datum label and confidence are given by h_{cls} and h_{conf} , respectively, whereas the noise label and confidence are given by $h_{\text{cls}} \circ \phi_T^{-1}$ and $h_{\text{conf}} \circ \phi_T^{-1}$, respectively.

The intuition behind the confidence-based filtering is that a datum (resp. seed) with lower confidence is more likely to lie near the boundary of a class region D_c (resp. Z_c). Consequently, a low-confidence seed is likely to produce a low-confidence denoised sample, which typically lies in a low-density region of the data distribution, where the score $\nabla \log p_t$ may become uncontrollably large. As noted above, trajectories initialized from such data may cause the probability-flow ODE to lose well-posedness, in particular, uniqueness. Consequently, one may expect sharp transitions of the diffusion model in neighborhoods of such seeds (Lobashev et al., 2025), making it difficult to predict the labels based on the seeds. We therefore propose the following methodology and experiments to study this effect.

4. Methodology

Motivated by the intuition that confidence plays a key role in predicting seed labels and revealing latent-space structure, we refine the two questions in Section 1 into the following more specific ones.

1. Can the label of a seed be predicted, and does it depend on its confidence?
2. Does the latent space restricted to different confidence level exhibits different structure?

To answer those questions we propose the following experimental framework.

1. **Predictability:** We generate random seeds and partition them into confidence levels for training and testing. For each level ℓ , we train a latent classifier $g_\ell : \mathbb{R}^d \rightarrow \mathbb{R}^C$ using seeds at that level and evaluate it on test sets across all confidence levels. Guided by Section 3.3, we expect classifiers trained on high-confidence seeds to achieve superior performance.

2. **Latent structure:** Seeds are similarly grouped by confidence level. Within the same level seeds are embedded using a supervised Linear Discriminant Analysis (LDA) projection followed by a nonlinear Uniform Manifold Approximation and Projection (UMAP). As suggested by Section 3.3, high-confidence seeds are expected to exhibit clear latent-class structure, whereas low-confidence seeds display more disordered patterns.

Next, we explain the role of the LDA–UMAP visualization pipeline, which we use throughout our experiments to study latent structure emergence.

Class-aligned projection via LDA. We use Linear Discriminant Analysis (LDA) as a supervised diagnostic projection to probe class-aligned structure in latent space. In our LDA–UMAP pipeline, LDA is not used as a classifier but rather as a linear projection that extracts directions maximizing between-class variance relative to within-class variance.

LDA projection is expected to reveal class-aligned separability when latent structure exists, whereas such separability will not emerge—even with labels provided—in the absence of latent structure. In Section 5, we observe that LDA yields strong separation only at high-confidence levels and collapses at low-confidence levels, despite using the same label information in both cases. This contrast indicates that the observed structure arises from the latent space itself rather than being an artifact of supervision.

Nonlinear visualization via LDA-UMAP pipeline. After the LDA projection, we apply UMAP to embed the noise vectors into two dimensions for visualization. UMAP is chosen for its ability to preserve local neighborhood structure and global topology in high-dimensional data.

As a control, we also apply UMAP directly to raw latent seeds. The direct UMAP produces no class-aligned structure across all confidence levels, indicating that the class-aligned structure is not directly accessible to UMAP in the raw latent space, thereby motivating the use of LDA as a supervised class-aligned projection.

5. Experiments and Results

We now present our main experimental results on predictability and latent-structure emergence across confidence levels. While our experiments focus on relatively small-scale datasets, this choice is intentional, enabling settings that are well understood and amenable to detailed analysis and providing an initial validation of the proposed framework. All experiments use the benchmark dataset in Section 5.1. We address the two questions from Section 4. For Question 1 (predictability), Section 5.2 begins with *Cross-Level Label Predictability*, which directly

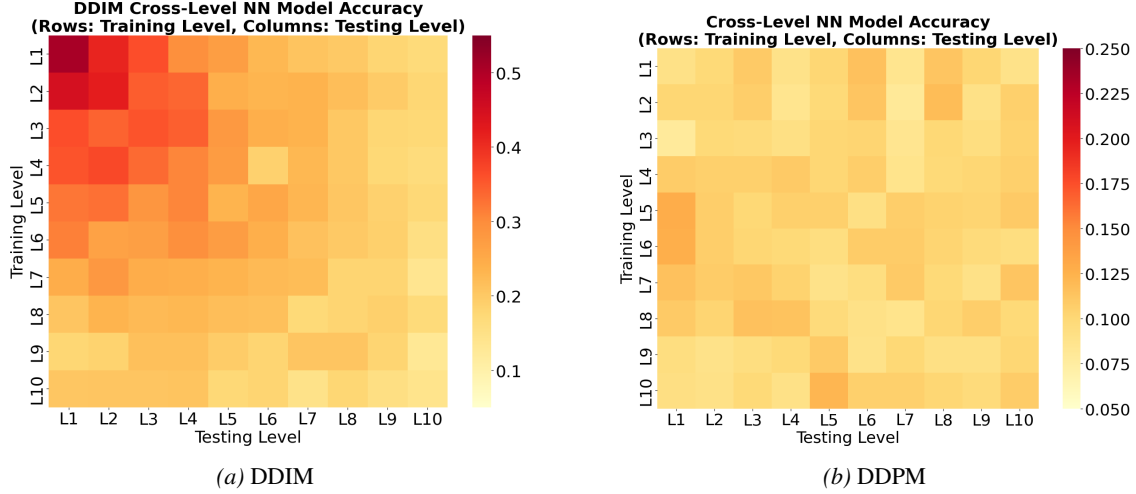


Figure 2. Cross-level classification accuracy heatmaps for diffusion noise across confidence levels through neural networks. **(a) DDIM:** A pronounced high-accuracy region appears in the high-confidence regime, indicating transferable predictability across levels (see Section B.1 for per-cell accuracies). **(b) DDPM:** Accuracy is heterogeneous across levels with no recognizable structure (see Section C for per-cell accuracies).

tests whether labels can be inferred from high-confidence noise, and is followed by *Accuracy vs. Predicted Confidence*, which evaluates confidence as a practical per-seed signal on newly sampled noise. For Question 2 (structure emergence), Section 5.3 starts with the core *LDA-UMAP* analysis that reveals nontrivial latent geometry in confidence-stratified noise, followed by ablations and diagnostics that further probe the observed structure.

5.1. Models and Benchmark Datasets

We use MNIST as the data distribution, a pretrained DDIM sampler as the diffusion model, and a LeNet-5 classifier trained on MNIST as the reference labeler. We construct a latent pool by drawing 70,000 i.i.d. Gaussian seeds from the standard normal latent distribution.

For each seed, we generate a denoised image using the diffusion model and evaluate it with the classifier, recording the predicted logit vector, label, and confidence. We then balance the dataset so that each label appears equally often, leaving 35,160 seeds.

To support confidence-controlled experiments, we stratify the balanced seeds into ten confidence levels. Concretely, within each label we sort seeds by confidence and split them into ten equal-sized bins; the ℓ -th global confidence level is formed by pooling the ℓ -th bin across all labels; We denote them by *level 1–level 10* (high to low confidence).

5.2. Predictability

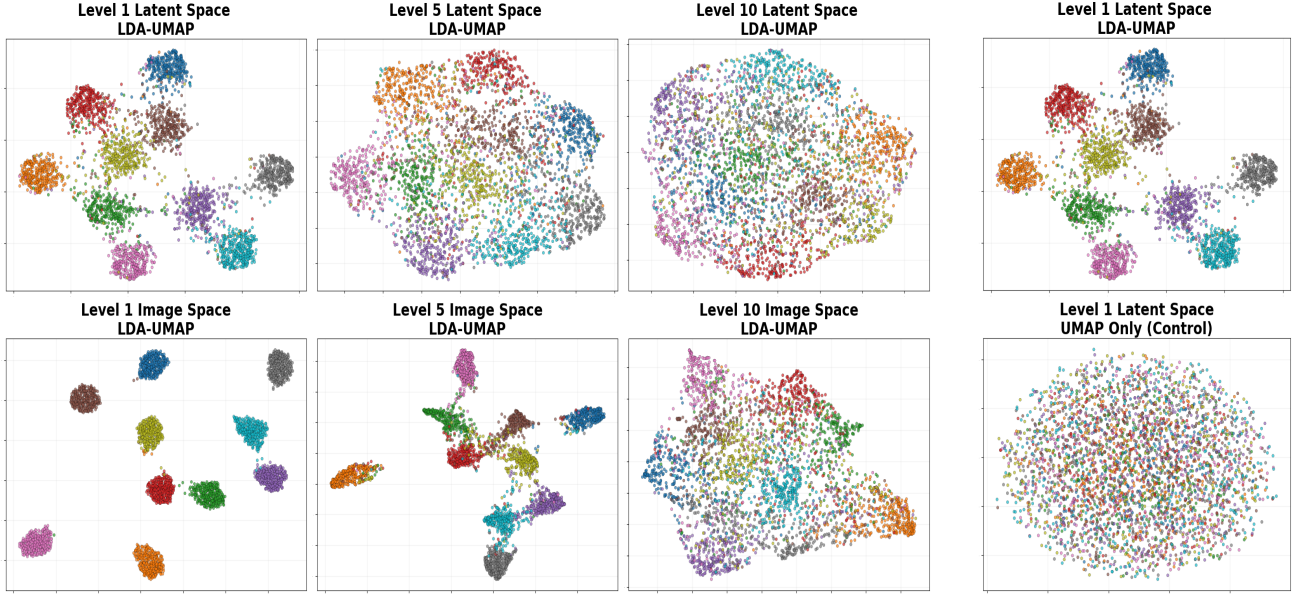
Cross-Level Label Predictability. We probe the fine structure of the leveled latent space via cross-level pre-

dictability. Using the stratified seed sets, we train a separate three-layer MLP (we found the lightweight architecture sufficient; deeper/wider networks yielded only marginal gains) on each confidence level and evaluate it on seeds from every level, yielding a full cross-level train–test accuracy matrix (shown in Figure 2a; more details in Section B.1).

The heatmap exhibits a pronounced high-accuracy region concentrated in the top-left corner, corresponding to training and testing on high-confidence noises. In contrast, accuracy degrades rapidly away from this region and becomes uniformly low and heterogeneous when either training or testing involves low-confidence levels. This suggests that meaningful, transferable structure is preserved primarily from high-confidence seeds, whereas low-confidence seeds provide little stable signal and exhibit a weak predictive structure. In comparison, Figure 2b shows the same experiment for DDPM-generated seeds, where no clear cross-level structure emerges, suggesting that increased stochasticity may obscure latent predictability.

Accuracy vs. Predicted Confidence (Logit Prediction). Motivated by the cross-level heatmap, which indicates that reliable prediction is concentrated in the high-confidence regime, we train a *logit-prediction* model using only the highest-confidence seeds. In this setting, the model takes a seed as input and predicts the classifier’s logits for the corresponding generated image; the predicted label and confidence are then derived from these logits via the argmax and the logit margin.

We then evaluate an accuracy–confidence diagnostic on newly sampled noise. Specifically, we draw 5,100 fresh seeds, use the trained model to output a label and confidence



(a) LDA-UMAP embeddings of latent seeds (top) and denoised images (bottom) across confidence levels. Both latent and image space exhibits class-aligned clustering at high confidence that degrades at lower confidence (see Section B.2 for embeddings of latent seeds across all confidence levels).

(b) UMAP-only shows no class-aligned structure while LDA-UMAP does.

Figure 3. Structure visualization via projection, with points colored by class label. **Left:** across confidence levels. **Right:** across methods.

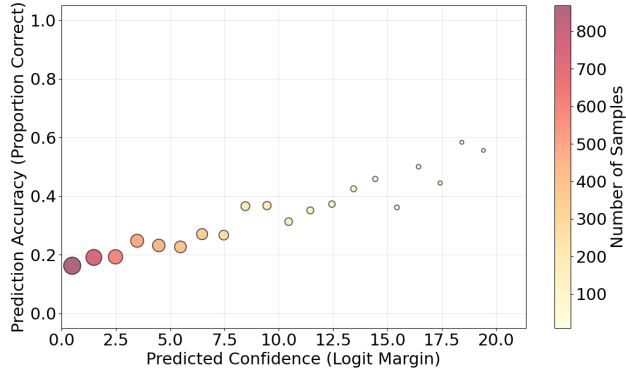


Figure 4. Prediction accuracy as a function of predicted confidence for the logit-prediction approach. Each point aggregates seeds within a confidence range; bubble size indicates the number of seeds in that bin.

for each seed, and denoise each seed to verify whether the predicted label matches the classifier label of the generated image. Figure 4 reports empirical accuracy as a function of predicted confidence.

As expected, accuracy increases monotonically with predicted confidence, while the lowest-confidence bins are both less reliable and more heavily populated. This supports using the predicted confidence as a practical, per-seed reliability signal when operating on randomly sampled noise. See Section E for additional details.

5.3. Latent Structure Emergence

Latent Structure via LDA-UMAP. With the LDA-UMAP pipeline introduced in Section 4, we examine the geometric organization of both latent seeds and denoised images across confidence levels to address Question 2. For each confidence level, latent seeds are projected via LDA from $\mathbb{R}^{28 \times 28}$ to a 9-dimensional subspace and then embedded into two dimensions using UMAP. Note that LDA is used only as a probing projection and not for prediction; if latent space lacked class-aligned structure, LDA would not induce meaningful separation, which is confirmed at low-confidence levels and by UMAP-only controls.

In Figure 3a, we compare latent-space and image-space embeddings. In the latent space (top row), Level 1 seeds exhibit clear class-aligned clustering, Level 5 seeds show degraded organization, and Level 10 seeds appear highly mixed. In contrast, the denoised image space (bottom row) exhibits weaker but still discernible class separation at Level 10, indicating that this geometric structure is intrinsic in image space but only partially and conditionally reflected in latent space. As a control, UMAP applied directly to raw latent seeds shows no class-aligned grouping (bottom of Figure 3b), indicating that class-aligned organization is not directly accessible in the raw latent space and that LDA serves as a class-aligned probing projection rather than a visualization artifact.

Figure 3 contrasts (i) confidence levels in latent space, (ii)

Table 1. LDA discriminability score and PCA variance explained by first 9 principal components across representative confidence levels.

Confidence Level	LDA Score (%)	PCA Variance(%)
Level 1 (High)	91.91	2.34
Level 5 (Medium)	77.40	2.31
Level 10 (Low)	65.63	2.31

latent and image-space geometry, and (iii) LDA–UMAP versus direct UMAP embeddings. Together, these comparisons indicate that latent structure is confidence-dependent rather than uniformly preserved by the diffusion flow.

Quantifying Structure Emergence. Beyond visualization, we quantify class-aligned structure using the *LDA discriminability score* (see Table 1), defined as the classification accuracy of an LDA model evaluated on held-out latent samples. This metric captures how well the LDA projection separates latent samples by class.

As a baseline, we compare this to the variance explained by a *9-dimensional PCA projection*. The dimension is chosen to match the one used in LDA for fair comparison. Here, the explained PCA variance refers to the fraction of total variance captured by the first 9 principal components; a higher variance indicates a more global geometric structure preserved by the PCA projection.

Table 1 shows that the LDA discriminability score decreases monotonically with confidence, indicating that class-aligned latent structure weakens at lower confidence levels. In contrast, the PCA variance explained remains nearly constant across confidence levels, suggesting that overall variance structure does not change with confidence. Hence, LDA provides a meaningful quantitative indicator for the strength of latent structure emergence.

Diffusive Nature of Low-Confidence Noises. Beyond the individual embeddings, we further examine how low-confidence noises are positioned relative to high-confidence structure. As shown in Figure 5, when Level 10 noises are overlaid onto the LDA–UMAP embedding learned from Level 1 noises, they do not form coherent clusters of their own. Instead, they predominantly populate interstitial regions between class-aligned Level 1 clusters, effectively filling the gaps between them. This suggests that low-confidence noises can be viewed as a diffuse extension of the high-confidence latent structure.

Comparison to Unconditional Latent Classifier. The results in Section 5.3 indicate substantial class-aligned geometric structure in the latent space \mathcal{Z} when conditioned by the confidence score. Now we provide some empirical ob-

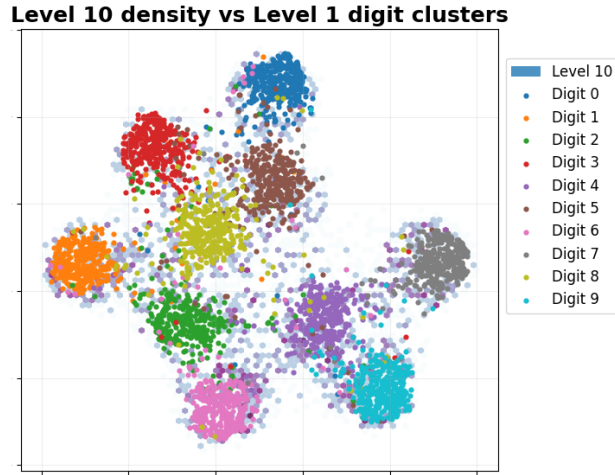


Figure 5. Overlay of low-confidence (Level 10) noises onto the LDA–UMAP embedding learned from high-confidence (Level 1) noises. While Level 1 samples form coherent class-aligned clusters, Level 10 noises do not form distinct groups and instead populate interstitial regions between these clusters.

servations on noises x sampled from \mathcal{Z} but not conditioned on confidence. While a model trained and tested on high-confidence noises can achieve a test accuracy of 53.42%, the same architecture trained and tested on the unconditional dataset exhibits substantially degraded performance (test accuracy 20.31%, F1 score 15.24%).

Furthermore, both the LDA discriminability score and the LDA–UMAP embeddings for unconditional noises are between those of Level 1 and the lowest confidence levels (See Appendix for more details). These observations suggest that while class-aligned structure exists in the latent space, it is diluted and only becomes defined after confidence-based filtering.

5.4. Summary of Predictability and Structure Emergence

Taken together, these results reveal a coherent picture of structure emergence in diffusion noise. The cross-level accuracy heatmap establishes partial label predictability in the latent space and characterizes how such predictability is shared across confidence levels. The LDA–UMAP visualizations further expose the class-aligned geometric organization, indicating a close relationship between label predictability and structure emergence in latent space.

In particular, high-confidence noise distributions exhibit mutually compatible and shared structure, whereas low-confidence distributions are more idiosyncratic and generalize poorly across levels. In this sense, **good noises are all alike, while bad noises are bad in their own ways**.

6. Implications and Analysis

Our experimental results not only demonstrate the feasibility of predicting labels from seeds, but also elucidate the underlying mechanism and provide an explicit prediction method. As a practical implication, this enables a conditional generation method as follows.

1. Given the diffusion generator and a data classifier, train a latent classifier on high-confidence seeds based on the classifier.
2. For conditional generation, sample seeds and retain those with both high confidence and the desired label. Generate sample based on those “good” seeds.

This approach differs fundamentally from standard guidance-based methods, as it treats the diffusion generator as a black box and requires neither modification nor retraining. Although our focus is on diffusion models, the proposed framework—including theory, experiments, and methodology—extends naturally to more general generative models, as it is largely agnostic to model architecture as long as the following assumptions are satisfied.

Assumption 6.1.

1. The generative model admits a deterministic generation process.
2. Either the generation process is invertible globally, or we have a method to identify the regions where the process is locally invertible.

The first and second impose explicit and implicit restrictions on the generative model, respectively. For diffusion models, DDPM violates the second assumption due to its inherent stochasticity, while the third assumption directs our attention to high-confidence regions and effectively disregards low-confidence ones.

Besides the assumptions, we would also like to list the strengths and limitations of our framework to assist future research or application based on our framework.

Strengths. Our framework is generator-agnostic and decouples conditioning from generation, enabling independent analysis and improvement of each component. It relies on objective class-based measures rather than subjective criteria that require costly human annotation. From a theoretical perspective, confidence-based filtering provides a new lens for latent-space analysis, revealing structure that becomes apparent only after appropriate preprocessing. Practically, the resulting conditional generation approach reduces sampling cost by carefully selecting seeds, often achieving high-quality outputs with few generations.

Limitations. Our framework assumes a deterministic generation process, which excludes stochastic samplers such as DDPM. Training the latent classifier can be computationally expensive, as it requires generating large numbers of seeds along with their corresponding samples and classifier logits across confidence levels and classes. While the LDA and UMAP visualizations demonstrate latent-class separability, they do not provide an explicit separating function. Finally, while Figure 4 empirically illustrates the distribution of seeds across confidence levels, we lack theoretical guarantees on the number of seeds required to obtain high-quality samples.

These limitations naturally motivate several directions for future work, as discussed in Section 7.

7. Discussion and Future Work

This work introduces a confidence-based framework for analyzing latent structure and enabling post-hoc conditional generation in diffusion models. While our results demonstrate the feasibility and effectiveness of the proposed approach in controlled settings, several directions remain open for future investigation.

A primary theoretical direction is to better understand the emergence of latent-class structure under confidence-based filtering. Our empirical findings suggest a close connection between confidence, invertibility of the generative map, and separability in latent space. Establishing formal guarantees on these relationships—such as conditions for separability, stability of latent flows, and the role of confidence in preventing mass concentration—would provide deeper insight into the mechanisms underlying our framework.

From a practical perspective, extending the framework beyond deterministic samplers to stochastic generation processes such as DDPM remains an important challenge. In addition, reducing the computational cost associated with training latent classifiers, for instance through more efficient seed sampling or adaptive selection strategies, would improve scalability. More broadly, the decoupling of conditioning and generation suggests that the proposed conditioning mechanism may serve as a flexible add-on to existing generative models without requiring architectural modification or retraining.

Overall, our results indicate that confidence plays a central role in revealing class-relevant structure in the latent space of diffusion models. By leveraging confidence-based filtering, we uncover latent structure that is otherwise obscured by the isotropic nature of the noise distribution and demonstrate its utility for post-hoc conditional generation. We hope this perspective encourages further investigation into latent-space analysis and principled conditioning mechanisms for generative models.

Acknowledgment

Wei Wei acknowledges funding from National Science Foundation under Grant DMS-2219384.

Impact Statement

This paper presents work whose goal is to advance the field of machine learning. There are many potential societal consequences of our work, none of which we feel must be specifically highlighted here.

References

Bradley, A. and Nakkiran, P. Classifier-free guidance is a predictor-corrector, 2024. URL <https://arxiv.org/abs/2408.09000>.

Castillo, A., Kohler, J., Pérez, J. C., Pérez, J. P., Pumarola, A., Ghanem, B., Arbeláez, P., and Thabet, A. Adaptive guidance: Training-free acceleration of conditional diffusion models, 2023. URL <https://arxiv.org/abs/2312.12487>.

Cho, W., Ravi, H., Harikumar, M., Khuc, V., Singh, K. K., Lu, J., Inouye, D., and Kale, A. Enhanced controllability of diffusion models via feature disentanglement and realism-enhanced sampling methods. In *Computer Vision – ECCV 2024: 18th European Conference, Milan, Italy, September 29–October 4, 2024, Proceedings, Part XXXVII*, pp. 285–301, Berlin, Heidelberg, 2024. Springer-Verlag. ISBN 978-3-031-72912-6. doi: 10.1007/978-3-031-72913-3_16. URL https://doi.org/10.1007/978-3-031-72913-3_16.

Chung, H., Kim, J., Park, G. Y., Nam, H., and Ye, J. C. Cfg++: Manifold-constrained classifier free guidance for diffusion models, 2024. URL <https://arxiv.org/abs/2406.08070>.

Dhariwal, P. and Nichol, A. Diffusion models beat gans on image synthesis. *Advances in neural information processing systems*, 34:8780–8794, 2021.

Ho, J. and Salimans, T. Classifier-free diffusion guidance. *arXiv preprint arXiv:2207.12598*, 2022.

Ho, J., Jain, A., and Abbeel, P. Denoising diffusion probabilistic models. In Larochelle, H., Ranzato, M., Hadsell, R., Balcan, M., and Lin, H. (eds.), *Advances in Neural Information Processing Systems*, volume 33, pp. 6840–6851. Curran Associates, Inc., 2020. URL https://proceedings.neurips.cc/paper_files/paper/2020/file/4c5bcfec8584af0d967f1ab10179ca4b-Paper.pdf.

Kim, D., Kim, Y., Kwon, S. J., Kang, W., and Moon, I.-C. Refining generative process with discriminator guidance in score-based diffusion models. In *Proceedings of the 40th International Conference on Machine Learning (ICML)*, volume 202, pp. 16567–16598. PMLR, 2023.

Kim, S., Kim, M., and Park, D. Test-time alignment of diffusion models without reward over-optimization. In *The Thirteenth International Conference on Learning Representations*, 2025. URL <https://openreview.net/forum?id=vi3DjUhFVm>.

Kirstain, Y., Polyak, A., Singer, U., Matiana, S., Penna, J., and Levy, O. Pick-a-pic: An open dataset of user preferences for text-to-image generation. In *Advances in Neural Information Processing Systems 36*, 2023.

Li, W., Xu, X., Xiao, X., Liu, J., Yang, H., Li, G., Wang, Z., Feng, Z., She, Q., Lyu, Y., and Wu, H. Upainting: Unified text-to-image diffusion generation with cross-modal guidance, 2022. URL <https://arxiv.org/abs/2210.16031>.

Lin, Z., Pathak, D., Li, B., Li, J., Xia, X., Neubig, G., Zhang, P., and Ramanan, D. Evaluating text-to-visual generation with image-to-text generation. In *Computer Vision – ECCV 2024: 18th European Conference, Proceedings, Part IX*, volume 15067 of *Lecture Notes in Computer Science*, pp. 366–384. Springer, 2024. doi: 10.1007/978-3-031-72673-6_20. URL <https://arxiv.org/abs/2404.01291>.

Lobashev, A., Guskov, D., Larchenko, M., and Tamm, M. Hessian geometry of latent space in generative models. In *Forty-second International Conference on Machine Learning*, 2025. URL <https://openreview.net/forum?id=H8JTsbG4KW>.

Na, B., Kim, Y., Park, M., Shin, D., Kang, W., and Moon, I.-C. Diffusion rejection sampling. In *Proceedings of the 41st International Conference on Machine Learning (ICML 2024)*, pp. 37097–37121. PMLR, 2024.

Nichol, A., Dhariwal, P., Ramesh, A., Shyam, P., Mishkin, P., McGrew, B., Sutskever, I., and Chen, M. Glide: Towards photorealistic image generation and editing with text-guided diffusion models. *arXiv preprint arXiv:2112.10741*, 2021.

Pavasovic, K. L., Verbeek, J., Biroli, G., and Mezard, M. Classifier-free guidance: From high-dimensional analysis to generalized guidance forms, 2025. URL <https://arxiv.org/abs/2502.07849>.

Preechakul, K., Chathee, N., Wizadwongsa, S., and Suwanjanakorn, S. Diffusion autoencoders: Toward a meaningful and decodable representation. In *Proceedings of the*

IEEE/CVF Conference on Computer Vision and Pattern Recognition (CVPR), pp. 10619–10629, June 2022.

Rombach, R., Blattmann, A., Lorenz, D., Esser, P., and Ommer, B. High-resolution image synthesis with latent diffusion models. In *Proceedings of the IEEE/CVF conference on computer vision and pattern recognition*, pp. 10684–10695, 2022.

Sohl-Dickstein, J., Weiss, E., Maheswaranathan, N., and Ganguli, S. Deep unsupervised learning using nonequilibrium thermodynamics. In Bach, F. and Blei, D. (eds.), *Proceedings of the 32nd International Conference on Machine Learning*, volume 37 of *Proceedings of Machine Learning Research*, pp. 2256–2265, Lille, France, 07–09 Jul 2015. PMLR. URL <https://proceedings.mlr.press/v37/sohl-dickstein15.html>.

Song, J., Meng, C., and Ermon, S. Denoising diffusion implicit models. In *International Conference on Learning Representations*, 2021. URL <https://openreview.net/forum?id=St1giarCHLP>.

Song, Y., Dhariwal, P., Chen, M., and Sutskever, I. Consistency models. In *Proceedings of the 40th International Conference on Machine Learning*, ICML’23. JMLR.org, 2023.

Wallace, B., Gokul, A., Ermon, S., and Naik, N. End-to-end diffusion latent optimization improves classifier guidance. In *Proceedings of the IEEE/CVF International Conference on Computer Vision*, pp. 7280–7290, 2023.

Xu, K., Zhang, L., and Shi, J. Good seed makes a good crop: Discovering secret seeds in text-to-image diffusion models. In *Proceedings of the IEEE/CVF Winter Conference on Applications of Computer Vision (WACV) 2025*, pp. 3024–3034, 2025. doi: 10.1109/WACV61041.2025.00299. URL <https://arxiv.org/abs/2405.14828>.

Yeh, P.-H., Lee, K.-H., and cheng Chen, J. Training-free diffusion model alignment with sampling demons. In *The Thirteenth International Conference on Learning Representations*, 2025. URL <https://openreview.net/forum?id=tFemqu1ED>.

A. Proofs of Theoretical Results

A.1. Proof of Theorem 3.1

Proof. For any open set $U \subset \mathbb{R}^d$, by the definition of probability flow, we have

$$\int_{\phi_t(U)} p_t(x) dx = \int_U p_0(x) dx. \quad (12)$$

Since $\phi_t : \mathbb{R}^d \rightarrow \mathbb{R}^d$ defines a homeomorphism, we apply the change of variable formula for the right hand side:

$$\int_U p_0(x) dx = \int_{\phi_t(U)} p_0(\phi_t^{-1}(x)) |\det(\nabla \phi_t^{-1}(x))| dx, \quad (13)$$

thus,

$$\int_{\phi_t(U)} p_t(x) dx = \int_{\phi_t(U)} p_0(\phi_t^{-1}(x)) |\det(\nabla \phi_t^{-1}(x))| dx. \quad (14)$$

Because U can be arbitrary, the above immediately implies

$$p_t(x) = p_0(\phi_t^{-1}(x)) |\det(\nabla \phi_t^{-1}(x))|. \quad (15)$$

□

A.2. Proof of Theorem 3.3

Proof. Since $\phi_T : \mathbb{R}^d \rightarrow \mathbb{R}$ is a homeomorphism, from the definition of data class and latent class, it is straightforward to see $Z = \cup_{c \in \mathcal{C}} Z_c$, with each Z_c connected and Z_c 's mutually disjoint.

By Theorem 3.1 and the definition of probability flow, we have

$$\begin{aligned} \mathcal{Z}(x|Z_c) &= \frac{\mathcal{Z}(x)}{\int_{Z_c} \mathcal{Z}(x) dx} \\ &= \frac{|\det(\nabla \phi_T^{-1}(x))| \mathcal{D}(\phi_T^{-1}(x))}{\int_{D_c = \phi_T^{-1}(Z_c)} \mathcal{D}(y) dy} \\ &= |\det(\nabla \phi_T^{-1}(x))| \mathcal{D}_c(\phi_T^{-1}(x)) = \mathcal{Z}_c(x). \end{aligned} \quad (16)$$

□

B. More Details on Experimental Results

This appendix provides supplementary details for Section 5.

B.1. Cross-Level Model Accuracy Heatmap

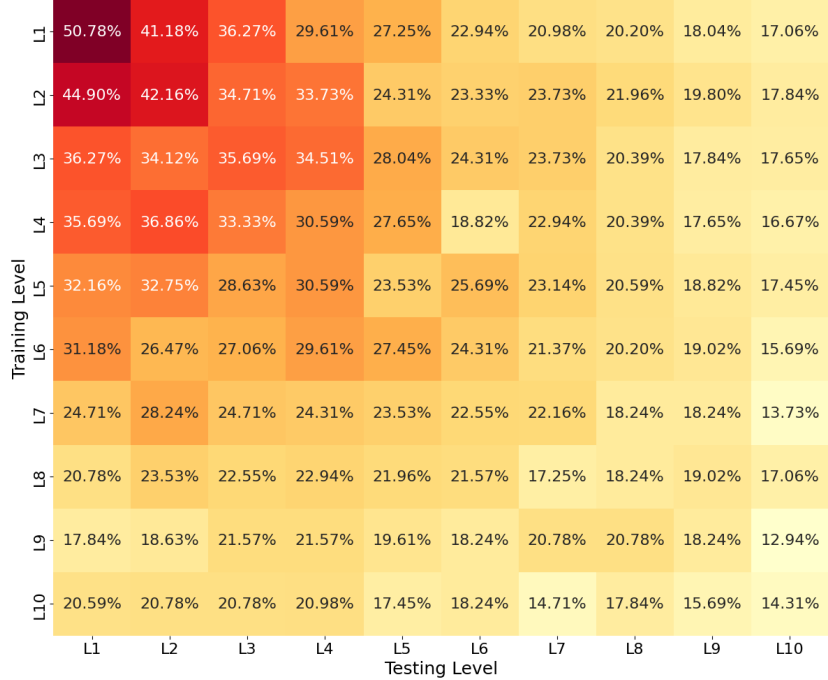
We report the full cross-level accuracy heatmap for Figure 2a with per-cell numeric values (See Figure 6a). We also include the corresponding heatmap obtained by replacing the MLP with an LDA classifier, which turns out almost identical, suggesting that the observed predictability is *intrinsic* rather than an artifact of the classifier choice (See Figure 6b).

B.2. LDA–UMAP Embedding

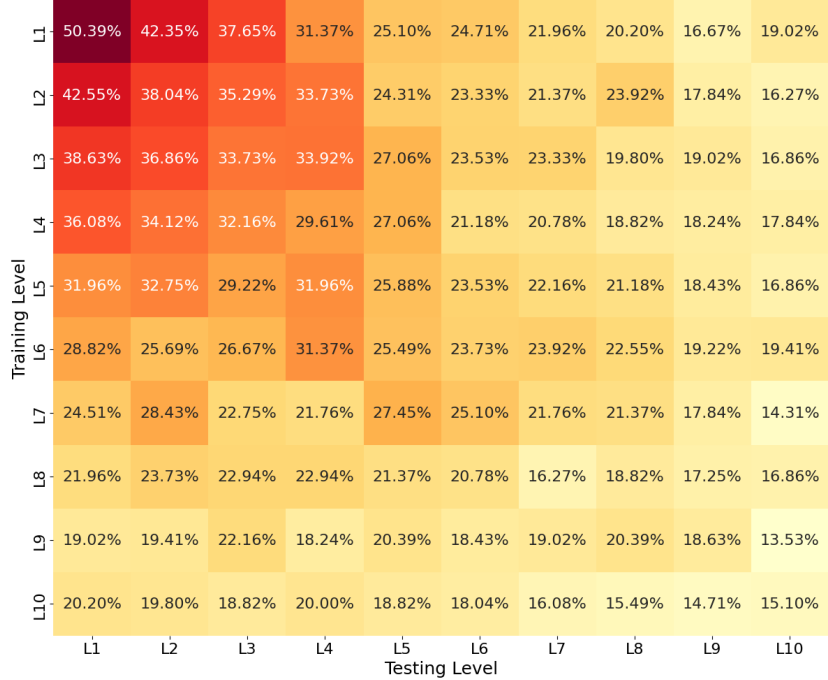
We include the full LDA–UMAP embedding of latent seeds across all confidence levels for Figure 3a, which reveals a smooth transition in latent geometry from ordered structure at high confidence to increasingly chaotic organization at low confidence (See Figure 7).

C. Latent Structure Disappearance with Stochastic Models

A deterministic sampler is essential for latent classification, since it induces a well-defined map from a seed to a generated sample (and hence to a label), making it meaningful to discuss latent structure. To validate this point, we repeat the



(a) Neural network model



(b) LDA model

Figure 6. Cross-level classification accuracy heatmaps for diffusion noise across confidence levels (with per-cell accuracies) through the (a) neural network model and (b) LDA model.

experiments in Section 5 after replacing DDIM with DDPM sampling. As anticipated, stochasticity breaks the seed-to-class correspondence: both the cross-level label predictability (Figure 2b, or Figure 8 for details) and the LDA–UMAP embeddings (Figure 9) collapse, showing neither stable transfer across confidence levels, nor coherent class separation. In short, under stochastic sampling, the latent structure becomes effectively unlearnable.

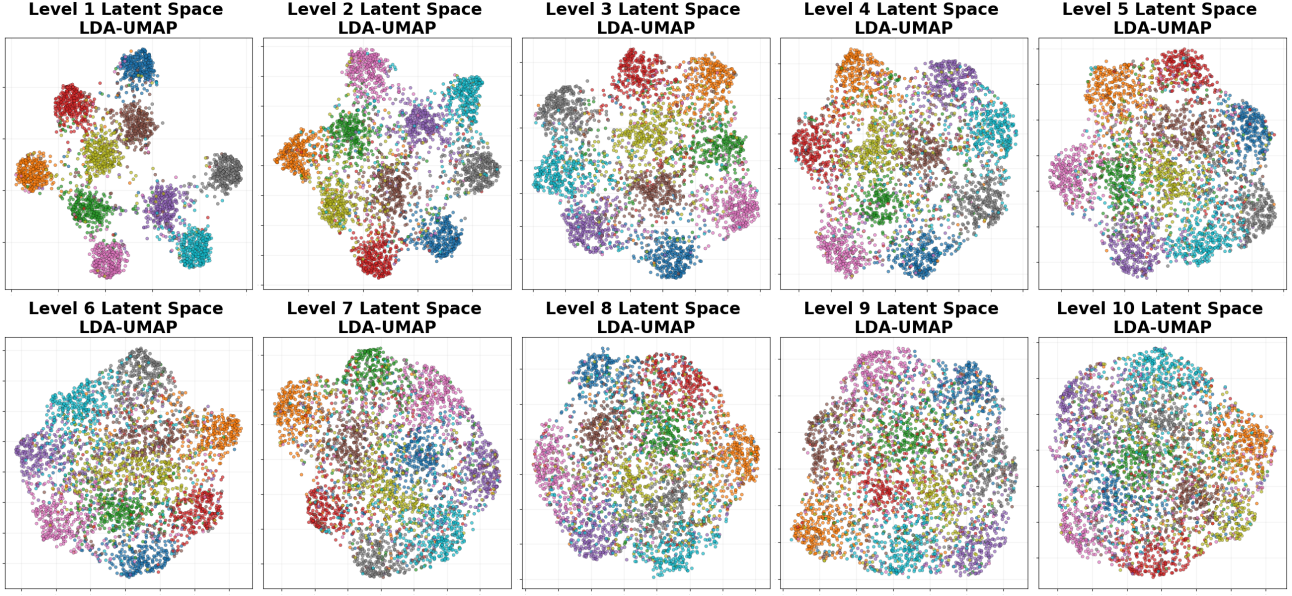


Figure 7. LDA-UMAP embeddings of latent seeds across all confidence levels.



(a) Neural network model

(b) LDA model

Figure 8. Cross-level classification accuracy heatmaps for diffusion noise across confidence levels (with per-cell accuracies) under DDPM setting through the (a) neural network model and (b) LDA model. Both models exhibit a heterogeneous accuracy across levels with no recognizable structure.

D. LDA-UMAP Pipeline on Denoised Images

We apply the LDA-UMAP pipeline introduced in Section 5 to images generated by the DDIM diffusion model. For each confidence level, we sample 3,500 denoised images, with 350 images per class label, yielding a balanced dataset across levels and classes.

As expected, denoised images exhibit strong intrinsic class-aligned clustering, with clustering strength decreasing as confidence levels drop. In this case, LDA-UMAP pipeline reveals class-aligned organization more clearly at lower confidence levels than UMAP alone, although both methods indicate degraded structure relative to high-confidence samples.

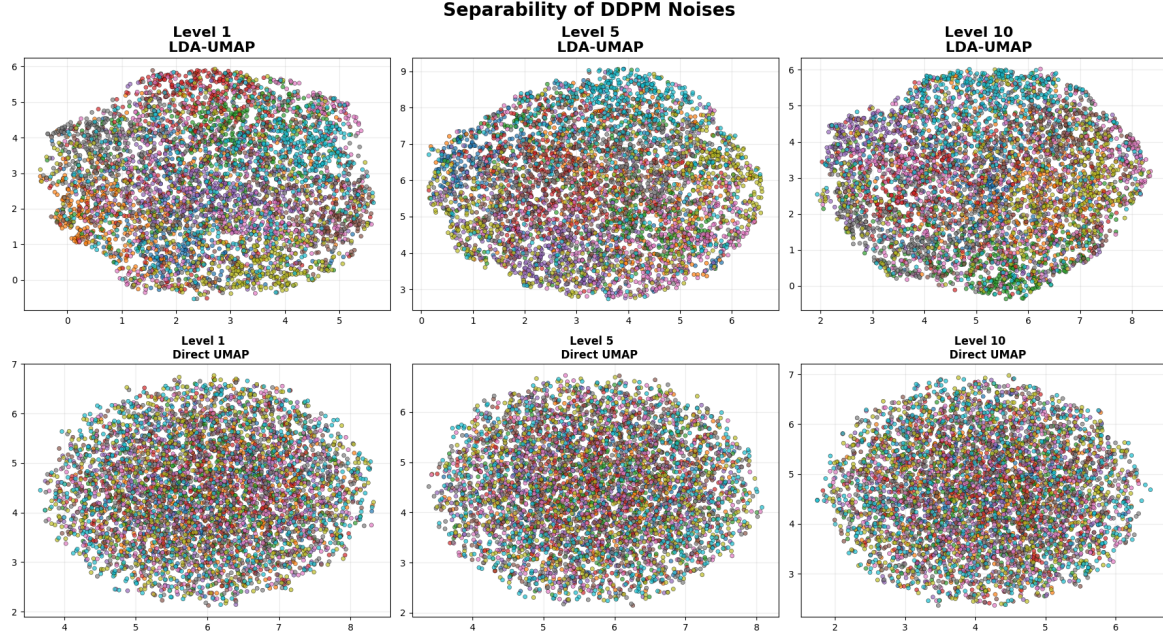


Figure 9. Separability in DDPM noises fails to appear under LDA-UMAP and UMAP only embedding.

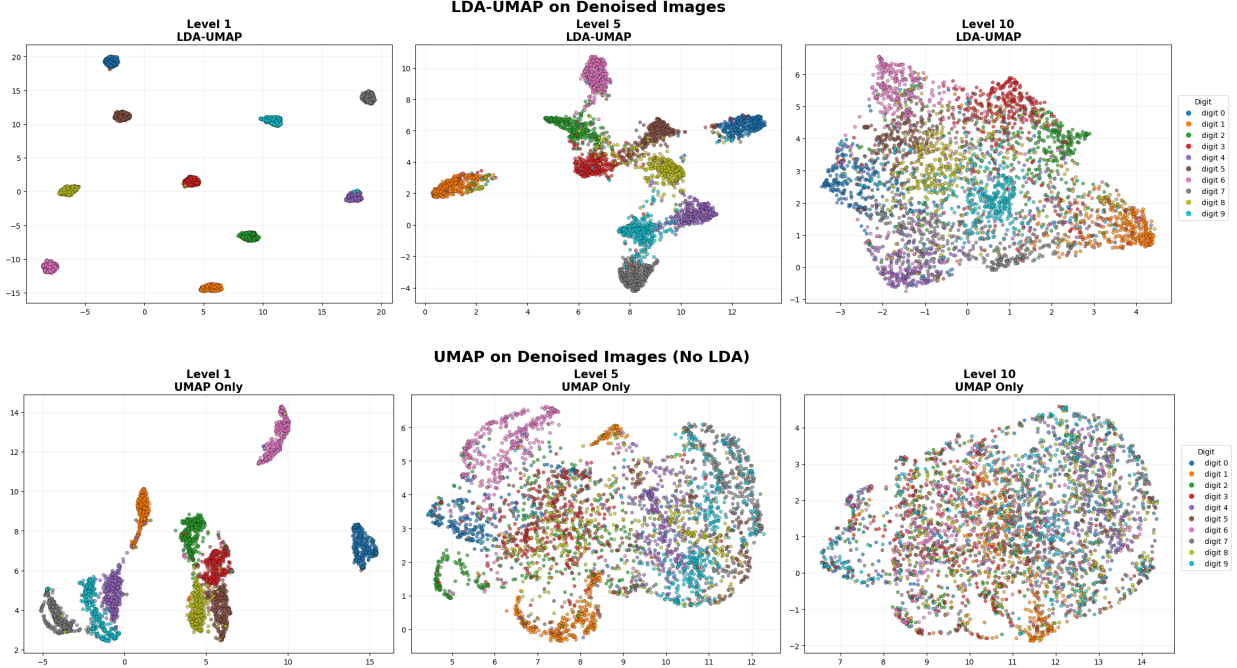
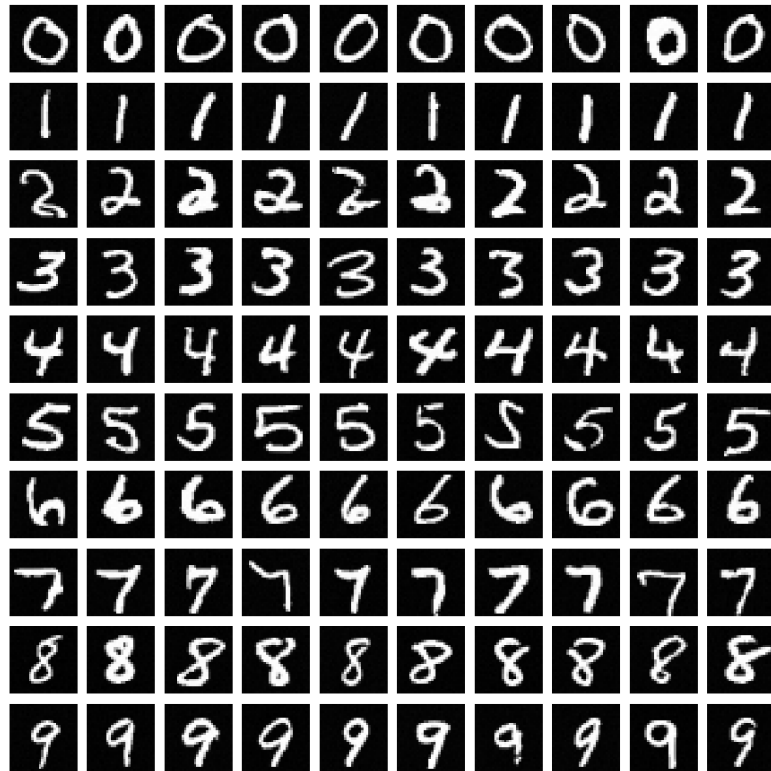


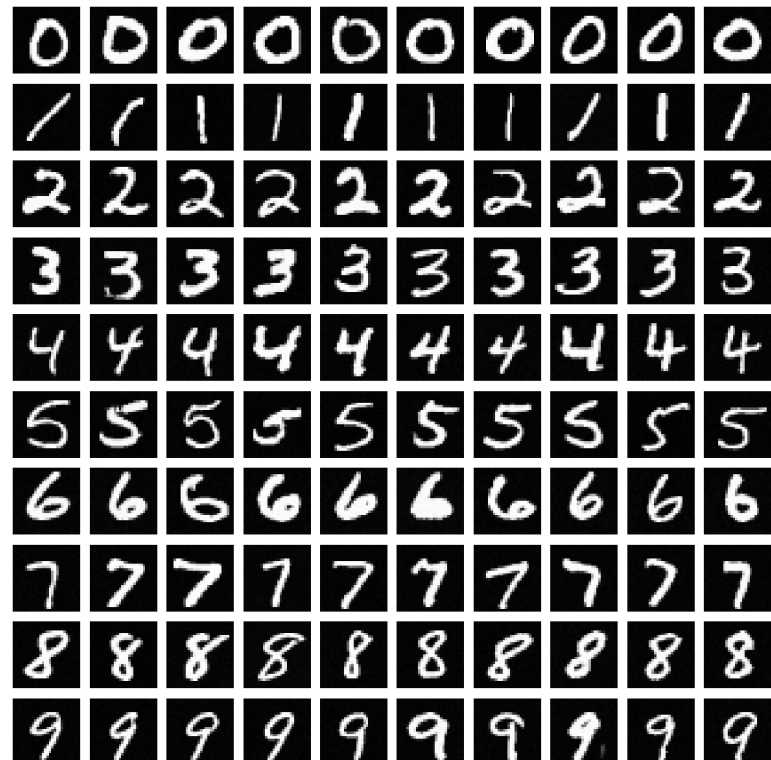
Figure 10. LDA-UMAP and UMAP-only embeddings of denoised DDIM images across confidence levels. Image space exhibits strong class-aligned clustering that weakens with decreasing confidence. LDA-UMAP reveals clearer separation at low confidence, while UMAP-only provides an unsupervised control.

E. Diversity in High-Confidence Seeds

Our *Accuracy vs. Predicted Confidence* pipeline in Section 5.2 conditions on high-confidence seeds (level 1). To verify that this selection does not collapse within-class diversity, we visualize the denoised samples per label generated from level 1 seeds and compare them with classifier-free guidance (CFG) targeting the same label.



(a) Within-class diversity from high-confidence (level 1) seeds under unconditional denoising (10 samples per label).



(b) Within-class diversity under (conditional) classifier-free guidance (CFG) (with guidance scale = 3) (10 samples per label).

Figure 11. Diversity comparison between confidence-based selection and classifier-free guidance.